Coarse-Grained Model of the Interaction of Light with Polymeric Material: Onset of Ablation

ARTICLE *in* THE JOURNAL OF PHYSICAL CHEMISTRY B · OCTOBER 2005

Impact Factor: 3.3 · DOI: 10.1021/jp0527711 · Source: PubMed

2 AUTHORS:

Yaroslava G Yingling
North Carolina State University
77 PUBLICATIONS **1,116** CITATIONS
SEE PROFILE

Barbara Garrison
Pennsylvania State University
368 PUBLICATIONS **9,434** CITATIONS
SEE PROFILE

Coarse-Grained Model of the Interaction of Light with Polymeric Material: Onset of Ablation

Yaroslava G. Yingling[†] and Barbara J. Garrison*

Department of Chemistry, 104 Chemistry Building, The Pennsylvania State University, University Park, Pennsylvania 16802

Received: May 25, 2005; In Final Form: July 7, 2005

A coarse-grained model has been developed for molecular dynamics simulations of the interaction of light with polymeric materials. The photon energy can result in a vibrational excitation (photothermal process) or disruption of a chemical bond (photochemical process) in a polymer. In the latter case, the formation of active radial sites and the occurrence of chemical reactions have to be taken into consideration. The novel feature of this model is the incorporation of chemical reactions into the united atom approximate representation of the polymer structure, which permits the study of laser ablation, degradation, or the effect of various chemical reactions on large time and length scales. The chemical reactions are included in the model in a probabilistic manner as in the kinetic Monte Carlo method. This model adopts physically and experimentally known quantities such as enthalpies and probabilities of reactions. Properties such as laser irradiation time, laser fluence, and wavelength are explicitly included. Moreover, no chemically correct interaction potential is required to incorporate the effects of chemical reactions on the dynamics of the system after energy deposition. We find that the model provides a plausible description of the essential processes. The laser-induced pressure relaxation is the main mechanism responsible for the onset of polymer ablation. Since the pressure relaxation processes are slow, there is a delay in the onset of ablation after the end of the laser pulse as is observed experimentally. The vaporization processes are not efficient for material removal, and the effect is minimal for both photochemical and photothermal processes. A lower fluence is needed for the onset of ablation with photochemical processes than photothermal processes.

Introduction

Ablation of polymers and biological tissues by far-UV lasers causes no apparent heat damage in the remaining sample presumably because most of the photon energy goes mostly into the breaking of chemical bonds, i.e., photochemical ablation, rather than heating the material, i.e., photothermal ablation.[1,2] Over the past two decades the materials that can be photochemically ablated have grown to include a number of commercial polymers, designer polymers, and biopolymers.[3] The industrial applications of photochemical ablation have expanded to generation of cylindrical holes in a highly integrated, multilayer printed circuit board,[4−6] drilling of ink jet nozzles,[3] stripping of polyurethane coating on wires,[7] direct writing of sub-100 nm features in polyimide,[8] fabrication of microfluidic devices, i.e., lab-on-a-chip,[9] creating designer polymers for fast fabrication of 3-dimensional topographies,[10] fabricating laser-driven microrockets,[11,12] and etching tissue in the corrective eye surgery LASIK.[13]

Despite the widespread development of the applications of UV irradiation of polymers, the mechanistic description of the processes involved in far-UV radiation of polymers remains fragmented. A paper by Lippert and Dickinson[14] delineates the following models: photochemical (direct bond breaking,[15−19] two-level model[20−22]), photothermal[23−27] (heat that breaks bonds), photophysical (direct bond breaking and heat),[28−32] photochemical surface,[33] photochemical volume,[15−18,34] thermal surface,[23,27,28,35] photothermal volume,[26,36] and volume photothermal.[37] Lippert and Dickinson point out that individual models describe particular experimental observations but none of the models are comprehensive in describing all of the experimental observations. Therefore, there is probably not one single mechanism that is important, but rather, a complex, intertwined array of events are occurring. There were many experimental[1−22,24−26,28,29,34−36] and computational studies[23,27,30−33,37−42] on laser ablation of various polymers conducted to elucidate the mechanism. Despite these studies, there are many questions remaining about the mechanism of material removal and the relative relevance of photochemical and photothermal processes.

Our group has developed and successfully applied the breathing sphere mesoscopic model[43,44] for use in molecular dynamics (MD) simulations of ablation of molecular solids commonly used in mass spectrometry. In addition, we have developed the coarse-grained chemical reaction model (CGCRM) for including chemical reactions in a united atom, bead and spring, or breathing sphere mesoscale simulation model.[45−47] The mesoscale approaches for modeling laser ablation of molecular solids have been quite successful in studying both photochemical and photothermal mechanisms of laser ablation, interpreting experimental data, and proposing new experiments.[44−46,48−51]

The advantage of these models is that none of the measured properties from the ablation experiments are used to fit any of the computational parameters. Rather, the parameters in the model are fit to a general set of mechanical, elastic, thermodynamic, and chemical properties of the system to be studied. The physical phenomena arise naturally out of the simulation; in particular, the formation of high laser-induced pressure, pressure wave propagation, phase explosion due to overheating,

* To whom correspondence should be addressed. E-mail: bjg@psu.edu.
[†] Currently at the Laboratory of Computational and Experimental Biology, Center for Cancer Research, National Cancer Institute, National Institutes of Health, Frederick, MD 21702.

10.1021/jp0527711 CCC: $30.25
Published on Web 08/05/2005

clusters in the plume, high ejection velocities, and spontaneous decomposition of the ablation plume are the effects observed in the simulations of molecular solids.[43,44,48,49] Similarly, the effects of the chemical reactions on the heat deposited in the system as well as the resulting compositional changes in the system are the results of the simulation rather than input quantities.[45−47] Entrainment of analyte molecules in the matrix is predicted by the simulations.[49,52,53] Moreover, the description of the material at a coarse-grained rather than atomic level makes it possible to model the time and length scales needed for the collective process of ablation. MD simulations provide complete information on molecular motions during and after the laser pulse, which makes it possible to compare the simulation results with a variety of experimental data.[44−46,49,54,55] The success of the prior simulations makes us optimistic about the extension of laser ablation simulations to more complex materials such as polymers and biological tissue.

In the present study, the CGCR model[47] is incorporated into a united atom mesoscale description of a polymer to examine the processes involved in ablation of polymers. To apply the CGCRM for ablation of polymers, a specific material is chosen, although we expect the insights into photothermal and photoablation of polymers to be general for a broad range of materials. As the model material, poly(methyl methacrylate) (PMMA) is chosen due to its straightforward photochemistry, available experimental and theoretical data for development of the model and comparison to results, and finally its extensive use in applications. PMMA is used for UV, electron, and X-ray lithography[56] and holography.[57,58] In lithography, PMMA is one of the highest resolution organic photoresists. With electron beam lithography, lines as narrow as 10 nm of PMMA can be produced.[57] Wider nodes of 70 and 100 nm of PMMA can be produced by lasers operating at 157, 193, and 248 nm wavelengths. A problem arises at the shorter wavelengths, however, as the polymer becomes too absorbent for practical use and it is believed that the photoproducts may outgas and condense on the exposure tool lens, degrading its transmission.[59] Due to the biocompatibility of PMMA with tissue, it is widely used in various medical applications. Bone cement PMMA is used commonly for fixation of prosthetics to bone or to anchor hip prostheses in the femur. The PMMA is later removed via laser irradiation during revision surgery.[60,61] Furthermore, PMMA is used for fabrication of microlens and -optical components with the laser ablation technique.[62−64] In pulsed laser deposition (PLD), PMMA films are used for deposition of a-C:H films.[65,66] Despite the plethora of applications, a complete fundamental understanding of the underlying processes of the interaction of laser radiation with PMMA does not exist.

In the following section, we give a detailed description of the model. The model is then applied to the investigation of the onset of photochemical and photothermal ablation of amorphous PMMA material, and the preliminary results of the model are presented. A summary of the work is given at the end.

Model

The goal of the modeling efforts is to assess the influence of the chemical reactions on the ablation phenomena, not to understand the details of a given reaction. A recently developed methodology (CGCRM) includes the effects of the reactions in molecular dynamics simulations in a probabilistic manner such as in a Monte Carlo calculation.[47] The essential pieces of information required are the enthalpies and dynamics/probabilities of reactions. In the previous studies, the CGCRM was successfully applied to a study of laser ablation of chlorobenzene via photochemical and photothermal mechanisms.[45,46]

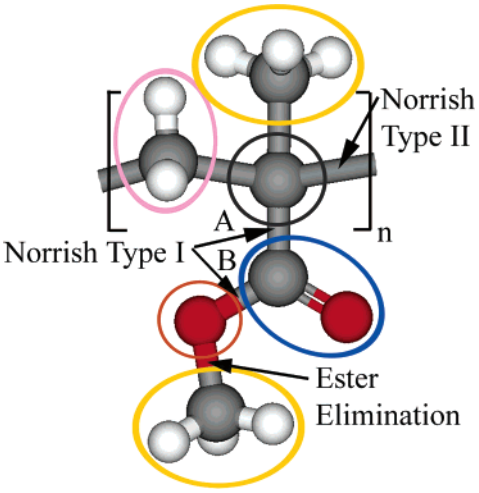

Figure 1. Representation of the PMMA coarse-grained scheme. Carbon atoms are gray, hydrogen atoms are white, and oxygen atoms are red. The ellipses represent approximations for the coarse-grained representation.

To model the laser irradiation of PMMA, we first need to understand the known photochemistry and the known experimental ablation observations. Second, a suitable coarse-grained description of PMMA and a means of generating the initial polymer sample must be developed. Third, a set of potential parameters needs to be chosen for each of the reactants, intermediate species, and products. Finally, a protocol, in this case the coarse-grained chemical reaction model, is needed to describe all the events that occur.

Photochemistry. PMMA has relatively straightforward photochemistry yet at the same time displays a wide range of important events for polymer ablation, such as bond scission, cross-linking, free radical reactions, and volatile gas formation. In addition, PMMA has been widely investigated in ablation studies, thus providing an experimental foundation for verification of our model.[67−69] Interaction of a high-energy photon with PMMA will result in one of three outcomes: main chain scission, side chain scission, or blocking group deprotection (Figure 1). Photon cleavage of the main chain bond (Norrish type II) leads to decomposition of the polymer into chains with lower molecular weight or even monomers. Photon cleavage at the ester carbonyl group (Norrish type I) results in the formation of carbon radicals on the main chain, thus leading to cross-linking of polymers as well as main chain scission and monomer elimination. The ester elimination reaction as well as the Norrish type I reaction can be followed by the loss of carbon dioxide or carbon monoxide.

The relative probability of particular chemical reactions involved depends on the wavelength. For instance, at 248 nm irradiation, the Norrish type I process dominates photochemical decomposition of PMMA.[67,70] At 248 nm, a relation of 1:6.25 between main chain and carboxyl decomposition was estimated,[28] whereas, at 157 nm, the Norrish type II reaction is believed to be dominant.[67] In addition to the photochemistry, the quantum yield, that is, the number of photons going into bond scission versus heat, and the absorption depth also depend on the wavelength. In conjunction with the chemical reactions and the change in the composition of the material, the absorption depth can also change with time. Finally, depending on the amount of heat deposited, temperature-activated reactions may occur. The interplay of all these effects is not understood.

Obviously, to build in all the chemistry described above in a detailed model is a significant undertaking. Thus, three representative processes that are important for irradiation of PMMA at 157 nm are chosen initially. These processes span the important types of events that transition photochemical ablation to photothermal ablation. The modeling steps include implementation of the chemical reactions in the coarse-grained MD simulation, choosing the appropriate interaction potentials reflecting the coarse-grained representation of PMMA, constructing an initial sample, and implementing the CGCRM methodology.

Reaction Protocols. *Photoinduced Bond Cleavage*. The bond-breaking event in the simulations such as a Norrish type II bond cleaved is effected by changing the particles corresponding to a bonding atom to a nonbonding one. There is a concomitant change in the interaction potential. We assume that the net repulsive interaction is about 1 eV above the bond dissociation energy. Thus, of the photon energy, 3.6 eV goes to breaking the chemical bond and ~1 eV goes toward further increasing the potential energy. The remaining photon energy is placed into thermal motion of the two fragments involved in the bond-breaking event. This protocol necessitates a threshold of about 4.6 eV for one-photon C−C bond cleavage. The other photon-induced bond cleavage processes[71] including activated release of CO and CO_2 will be handled in a similar manner.

Thermally Activated Unzipping from a Radical. We assume that the polymer can unzip from a radical along the backbone, eliminating one monomer at a time. For a change in energy of ΔE, the rate, k, can be approximated by

$$k = \upsilon \exp(-\Delta E/k_B T)$$

where $\upsilon \approx 10^{13}\ s^{-1}$. The lifetime of a radical, τ, is given by the reciprocal of the rate constant or

$$\tau = (1/\upsilon) \exp(\Delta E/k_B T)$$

The temperature, T, will be determined from the kinetic energy of the monomer with the radical site where the unzipping can occur. Stoliarov et al. calculate the enthalpy change to be endothermic by 91 kJ/mol or approximately 0.94 eV/monomer.[42] This value corresponds to having a previous broken chain with a radical end and removing one monomer unit. The net effect is to break one C−C single bond and create a double bond. Since the unzipping of a monomer is endothermic, there will be a concomitant decrease in the kinetic energy of the neighboring particles.

Formation of a Monomer. A monomer may form from either the unzipping reaction or another photon absorption event. A double bond of strength 6.36 eV is formed in the monomer. The potential energy change due to the double bond formation will be offset by a comparable increase in kinetic energy of the monomer.

Cross-Linking. The cross-linking reaction between radicals on different polymer chains will be accommodated by replacing radical interaction potentials with the bonding potential. There will be a concomitant gain in heat (kinetic energy) as the potential energy of the system is lowered due to the bond formation.

Deposition of Heat. For deposition of the photon energy as heat, the kinetic energy of the particles in one randomly chosen monomer will be adjusted to increase the energy of the system by an amount equal to the photon energy.

Coarse-Grained Model of PMMA. The choice for the united atom approximation in PMMA is based on the photochemistry described in the previous section. As shown in Figure 1, the PMMA monomer is described as a branched molecule with C, CH_2, CH_3, CO, and O particles. The polymer structure retains the bond angles and lengths of the original molecule. With this particular choice of coarse-grained representation, the proposed reaction products mentioned above can be described. With this choice of coarse-grained representation the computationally intensive explicit H atoms and C=O double bond have been eliminated.

TABLE 1: Bond Stretch Parameters

bond	D_e (eV)	r_0 (Å)	k_{str} (eV/Å^2)	α (Å^{-1})	r_{str} (Å)
C−CH_3	3.8	2.64	14.36	1.94	2.71
C−CH_2	3.6	1.54	14.36	1.99	1.63
C−CO	3.6	1.49	14.36	1.99	1.58
OC−O	3.5	1.34	15.29	2.1	1.44
O−CH_3	3.5	2.59	15.29	2.1	2.68

Interaction Potentials. The potential energy (U) of the system includes terms describing the interactions due to bonds between particles, angle bend interactions along the chain, and nonbonding long-ranged interactions between particles on different chains and between particles on the same chain. The goal is to model the dynamical effects of laser ablation with the inclusion of reactions as described above; thus, some adaptations have been made to conventional approaches for the potentials to best accommodate the CGCRM. In all cases, the objective is to include the essential interactions, to have the correct cohesive energy and density of PMMA, and to predict reasonably the glass transition temperature.

Bonding Interactions. Bond stretch and bond angle bend interactions for hydrocarbon systems are well established and are often expressed in terms of the harmonic approximation. The challenge for our simulations is that we need to be able to break bonds if the system gets sufficiently hot or sufficiently strained during the ablation conditions. To account for fracture of the bond, the hybrid model[72] is used where the bonds exhibit elastic behavior for displacements from equilibrium until the bond length reaches a critical value l_c where a Morse-type potential is applied:

$$U_{str}(r) = \{k_{str}(r - r_0)^2 - D_e\} \quad \text{for} \quad r \le r_{str}$$

$$U_{str}(r) = \{D_e[\exp(-2\alpha(r - r_0)) - 2\exp(-\alpha(r - r_0))] + \Delta U\} \quad \text{for} \quad r > r_{str}$$

with

$$\Delta U = \{k_{str}(r_{str} - r_0)^2 - D_e[1 + \exp(-2\alpha(r_{str} - r_0)) - 2\exp(-\alpha(r_{str} - r_0))]\}$$

The parameters for these harmonic and Morse potentials are fit to those used in atomistic calculations[73,74] and are given in Table 1.

The primary angular interaction is the bond angle bend motion. Torsional interactions are important for equilibrium configurations and motions near equilibrium but are not as important for the ablation dynamics. The angle bend term is assumed to be harmonic:

$$U_{bend}(\theta) = k_{ang}(\theta - \theta_0)^2$$

The potential parameters are also fit to those used in atomistic calculations[73,74] and are given in Table 2. The harmonic angle bend potential does not dissociate; thus, when two particles

TABLE 2: Angle Bend Parameters

angle	θ_0 (deg)	k_{ang} (eV/deg^2)
C−C−C	109.0	2.02
C−CO−O	117.0	2.95
CO−O−CH_3	124.0	2.6

dissociate, the associated angle bend terms are simply removed. Changes in energy due to the discontinuity in this potential are adjusted by altering the kinetic energy when particles are transformed.

Long-Range Interactions. Typically, for long-range interactions a site−site model is used to describe the potential between a pair of atoms. Within this description, there are parameters for the interaction for each pair of particle types. For these simulations of laser ablation of organic solids, an alternative to this description was proposed in which the interaction between a pair of particles is evaluated from the edge of the particles.[43,44] The rationale for this choice is that the interaction between a pair of molecules is dominated by the outer functional groups and not portions of the molecule buried inside. Moreover, heterogeneous materials such as large analyte molecules embedded in matrix molecules can be easily accommodated.[43,52,53,55] Within this description each particle, i, is assigned a radius, R_i. The appropriate distance for evaluating the potential between particles i and j is $r_{ij} - R_i - R_j - R_e$, where r_{ij} is the center-to-center (or site-to-site) distance and R_e is the equilibrium distance between the edges of the particles. The conveniences of this choice for the original breathing sphere model are straightforward.[43] First, changes in the internal energy of a molecule, e.g., from an absorption of a photon, results in changes in the radius; consequently, there can be energy transfer from one molecule to the next. Second, there is only one set of potential parameters for all the species with only the radii being different.

This style of description between nonbonding pairs of particles is continued for the simulations of laser ablation of polymers even though breathing spheres are not being used. We feel that this choice is particularly convenient for breaking a bond and changing, for example, a bonding C site to a radical C site. The radius (size) of this carbon site can increase, and the interaction is intuitively more repulsive. Moreover, at a later time, if it is appropriate, then it is possible to reintroduce the breathing spheres.

Following the previous work, a Morse potential is chosen for the interaction between a pair of particles. We realize that a Lennard-Jones potential is conventionally chosen for long-range interactions but the Morse potential affords us the additional parameter, α, that influences the repulsive wall of the potential. The goal is to model the dynamics of ablation rather than the precise equilibrium structure; thus, this choice is acceptable. Specifically, the Morse potential is given by

$$U_{\text{nonbonding}}(r_{ij}) = D_e(1 - \exp(-\alpha(r_{ij} - R_i - R_j - R_e))^2 - D_e$$

Within this description, the well-depth, D_e, α, and R_e are the same for all pairs of interactions, 0.03 eV, 1.0 Å^{-1}, and 1.8 Å, respectively. As discussed below, these parameters were obtained from simulations aimed at reproducing the cohesive energy, density, and glass transition temperature of PMMA. A cutoff distance of 10 Å for the edge-to-edge distance is used.

This nonbonding potential is used for all pairs of particles from different polymer chains as well as particles that are separated by at least four neighbors in a given chain. The (1,4) interactions within a chain are typically described by a torsional term that, as explained above, we are ignoring. The radii of the particles in the bonded polymer chain are taken from theoretical estimates[75] and are given in Table 3 along with the masses of the particles.

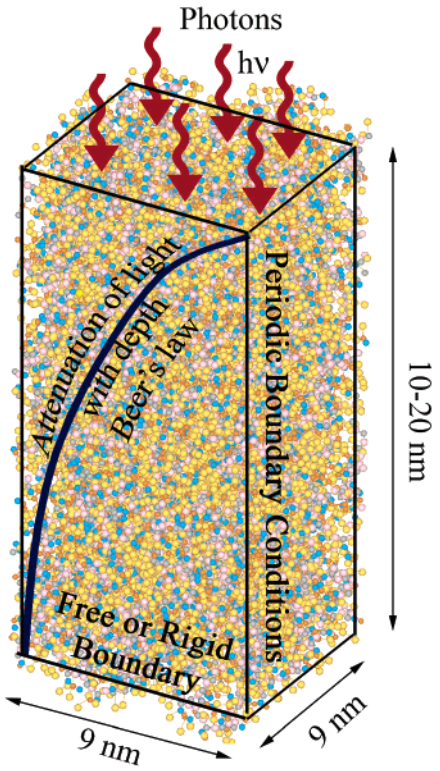

Figure 2. Computational setup. The colors are assigned by bead type with the same colors as the circles in Figure 1.

TABLE 3: United Atom Particle Properties

	C	CH_2	CH_3	CO	O
mass, Da	12.01	14.026	15.034	28.01	16.00
radius,[75] Å	1.61	1.88	1.88	1.60	1.42

The remaining challenge is to determine the radii of the radical species. The choice of parameters must be such that the replacements of particles described above can be made and that the correct energy change of the reactions can be implemented. Since the reactions can occur when the system is in the solid, liquid, or gaseous phase, numerous simulations need to be performed to test the potentials.[45,47] To date we have determined potential parameters for the C, CH_2, and terminal CH_3 radicals. The radius of the radical is 2% larger than the radius for the bonding configuration, and the value of α is 20% larger.

Simulation Setup. The laser irradiation of the system is simulated by randomly choosing the particle(s) to absorb the photon and the type of event to occur (bond cleavage or heat deposition) on the basis of a chosen quantum yield. The total number of photons entering the model during the laser pulse is determined by the laser fluence. The absorption probability is modulated by Beer's law to reproduce the exponential attenuation of the laser light with depth. The absorption probability can depend on the reaction event, e.g., Norrish type I or II bond cleavage, or can change with time with material composition changes. The photons are absorbed by the system during a prescribed time; thus, the effects of different laser pulse widths can be assessed. The events in the center of the laser beam are modeled; thus, periodic boundary conditions are used in the two horizontal directions as shown schematically in Figure 2. To accommodate the material removal in the upward direction and

the pressure pulse into the solid, the sample is typically much deeper than it is wide.

The length of the longest polymer in the sample strictly depends on the minimum horizontal dimension, due to the periodic boundary conditions. On the basis of the density, the polymers are placed in the sample accordingly by propagation of a polymer chain grown step by step into the lowest density region via a self-avoiding Monte Carlo random walk. When the polymer chain reaches the side, it automatically reenters through the opposite face due to the periodic boundary conditions. This self-avoiding walk is performed with only knowledge of the bond lengths between particles and bond angles and not the specific interaction potential. The sample can be easily converted, for example, to poly(dihydrofluorooctylacrylate) or other polymers with a similar coarse-grained structure.

After generation of the sample, simulated annealing calculations were performed both for equilibrating the sample and for determining the parameters in the long-range potential. Beginning with MD simulations at a constant pressure of 1 atm and a constant temperature of 600 K, the sample is then quenched. This protocol is repeated with different potential parameters until the predicted properties of the atactic PMMA are as follows: density of 1.19 g/cm^3, cohesive energy per monomer (MMA) equal to 0.53 eV, and glass transition temperature equal to 395 K.[73] The potential parameters and radii for the radicals are established with a similar protocol.

The sample size used in this study is 5 nm $\times$ 5 nm $\times$ 13.6 nm and contains 135 polymers with 13 MMA monomers or 79 particles each. The total number of particles in the sample is about 10665. A penetration depth of 8 nm is used. Laser pulses of 5, 15, and 50 ps in duration at a wavelength of 157 nm (7.98 eV) are used in the simulations. A Nordsieck predictor−corrector is used to integrate the equation of motions with a time step of 2 fs. This choice of the relatively short wavelength is to limit the reaction events to only the Norrish type II process. Similarly, picosecond pulses are used rather than the experimental nanosecond pulses due to issues associated with the pressure wave as discussed in the next paragraph.

The reflection of the pressure wave from the bottom of the sample leads to the cracking of the sample and dramatic increase of the yield.[76] Therefore, to avoid artifacts of the pressure reflection, the analysis of the simulations is stopped as soon as the pressure wave reaches the bottom. Thus, the simulations here describe the onset of the ablation process. Development of appropriate boundary conditions is ongoing to extend the time of the simulations, perform more detailed and realistic studies, and compare yields and plume compositions to experimental observations.

Coarse-Grained Chemical Reaction Model for Photoablation of Polymers. The essence of the proposed approach for modeling photoablation of polymers has been piecewise described in the previous text. The protocol is to perform a molecular dynamics simulation using a mesoscale or coarse-grained representation of the system. A set of conditions is established for which chemical reactions can occur during the simulation. If these conditions are met, covalent bonds between particles are allowed to break or form. Each reaction event is accomplished by removing the reactant particles and replacing them with the product particles. This replacement is accompanied by changes in the interaction potential. For each reaction event, the energy change of the system is the appropriate reaction enthalpy. This protocol is best described for the conditions when there are radical sites present. The steps for incorporating chemical reactions in the simulation proceed as follows. (1) Track all reactive species, in this case, each radical and its associated monomer. (2) After each 2 fs time step, check the vicinity of each reactive species for possible reaction partners, i.e., cross-linking, and check the temperature of the surroundings for thermal unzipping. (a) If two radicals are within 3 Å of each other, create the covalent bond between radicals by switching the potential functions. (b) If the temperature of the MMA monomer with the radical site is higher than the unzipping activation temperature, break the C−CH_2 bond by removing the covalent potential and replacing it with the radical potentials and create a double bond instead of a single bond by switching the potentials within the monomer. As a result, a new radical site is created on a polymer chain and MMA is formed. (3) The deposition of energy change is carefully monitored so that the total energy change of the system is the enthalpy of the reaction. (4) Integrate the particles in the regions where reactions are taking place with a reduced time step to partially equilibrate the positions. In the simulations, the local region is integrated for 10 time steps at one-tenth the normal time step of the whole simulation. For the duration of the laser pulse, the same protocol is implemented except that every few steps, depending on the fluence, a photon is absorbed into one of the allowed channels.

The simulations of photothermal and photochemical ablation of polymers are designed to model the ablation process and to assess the effect and interplay of the various physical and chemical processes on the measurable quantities. The simulations are not designed, however, to predict the fundamental chemical reactions of the polymer, for example, the Norrish reactions. Similarly, absorption coefficients (or penetration depths) that change with composition can be implemented into the model, but the model is not able to predict the quantitative changes in penetration depth. The simulations as proposed consider only neutral species; thus, no ions can be predicted at this time although the CGCR model is sufficiently flexible to include them in the future. Even though it might be desirable to predict the chemical reactions and the ionic processes, it is clear that significant insight can be gained into the ablation dynamics of polymers without these effects. Finally, although these simulations make significant progress in approaching the experimental time and length scales, they are not quite the same as in experiment. On the basis of our experience in modeling laser ablation of organic solids, the simulations nonetheless provide illuminating insights into the ablation events.

Results and Discussion

A series of molecular dynamics simulations of laser ablation at several fluences and laser pulse durations were performed on a coarse-grained amorphous PMMA sample to examine the onset of ablation. We start with discussion of the laser ablation initiated by photochemical processes, in particular main chain scission (Norrish type II reaction). A fluence of 0.3 mJ/cm^2 and pulse duration of 50 ps are chosen as the system shows clear evidence of the ablation process. Four snapshots of the plume are shown in Figure 3. A total of 59 photons were absorbed by the material, which resulted in 59 photochemically broken backbone bonds and simultaneous creation of reaction products. At this fluence a small number of particles, mostly terminal CH_3 groups, are desorbed by the end of the laser pulse at 50 ps. At 60 ps there are many more fragments of the polymers in the plume, representing the onset of ablation. At 70 ps, the yield has dramatically increased and even some intact polymers are ejected from the material. The increase in the number of pieces of polymer as indicated by the increase in colors in going from

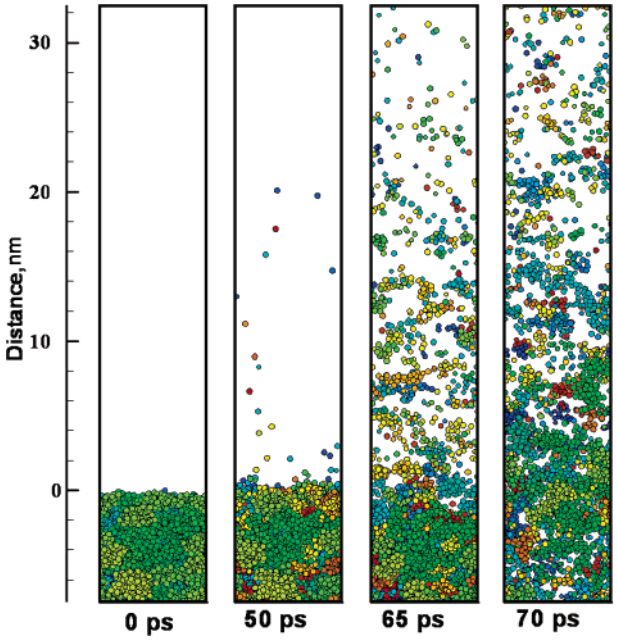

Figure 3. Snapshots from MD simulation of laser ablation of PMMA initiated by pure photochemical processes: laser fluence 0.3 mJ/cm^2 (59 photons), penetration depth 8 nm, pulse duration 50 ps. Each color designates a different piece of polymer. Initially all the chains are shades of green or blue. The larger diversity of color for the photochemical ablation signifies that more bonds have been broken.

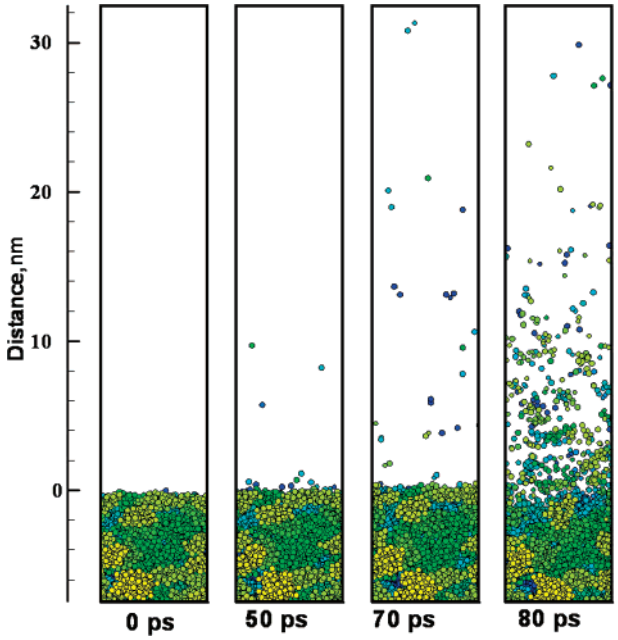

Figure 4. Snapshots from MD simulation of laser ablation of PMMA initiated by pure photothermal processes. The conditions are the same as in Figure 3 except the laser fluence is 0.5 mJ/cm^2 (98 photons).

50 to 70 ps indicates that bond cleavages continue well beyond the end of the laser pulse.

The physical properties and concepts that have been used to describe ablation of molecular organic solids include the cohesive energy of the material and pressure buildup.[43,44] Conceptually, the cohesive energy is related to the energy needed to vaporize a particle. In the case of polymers, however, the definition of cohesive energy with respect to ablation is intricate. The average cohesive energy in the simulations is 0.53 eV per MMA unit. Each MMA, however, has one (end unit) or two covalent bonds of strength 3.6 eV which connect it to the polymer. Thus, the energy required to remove a species from the solid depends on the length of the polymer chain or fragment and whether a bond or two must be broken before it desorbs. To complicate the matter, most of the polymers are intertwined with each other and are not simply lying on the surface. Throughout the simulations five MMA units are created; however, most of the formed MMA is not located on the surface and, therefore, is not present in the plume.

The pressure in the system is the driving force for the ablation process. Part of the pressure buildup arises from the increase in size of the photofragments relative to the species bound in the polymer.[77] The other contributor to the pressure buildup is the excess energy above the bond cleavage energy that goes into the heat of the surroundings. During laser excitation, the increase in thermal energy of the material would normally lead to thermal expansion.[44] The thermal expansion in polymers during the laser pulse is minimal (Figure 3); therefore, heating of the material is taking place at nearly constant volume. The result of such heating is a high-pressure buildup in the absorbing region. The high pressure can relax by expansion of the material, leading to acceleration of the material away from the surface in the surface region and to the propagation of a strong compression wave into the bottom of the sample.[44] Ablation is initiated when these forces exceed the strength of the material and cause polymer fracture and subsequently ejection. In these simulations, the pressure is relatively strong, peaking at 100 MPa. The propagation of the pressure wave and thus the relaxation of the pressure, however, are slow because the polymers are intertwined and interconnected with strong covalent bonds. This delay in the pressure relaxation delays the ablation event to after the end of the laser pulse as seen in Figure 3 at 65 and 70 ps. Therefore, for polymer ablation the laser-induced pressure relaxation is the main mechanism responsible for the onset of ablations, the vaporization processes are not efficient, and the effect is minimal. The single beads presented in the plume are due to overheating of the material, however, since heating proceeds in parallel with the pressure-driven ablation.

The ablation, however, can be initiated at energy densities much lower than those required for vaporization due to the occurrence of photomechanical effects caused by laser-induced stresses.[44] In our simulations the onset of ablation is delayed after the laser pulse and started at about 60 ps as can be seen in Figure 3. The rapid increase in yield represents the onset of ablation. There is a clear change in the structure of the ejected plume at 65 ps. There are more beads and bigger chunks of polymers ejected from the surface than when the laser is on.

The photothermal processes are modeled by putting the full photon energy into the sample as heat as shown in Figure 4. Since the bonds are not broken directly by the photons, more energy is needed for ablation, and thus, a fluence of 0.5 mJ/cm^2 corresponding to 98 photons is used. At the end of the pulse, the deposited heat is almost 3 times higher than in the simulation of the photochemical process. The state of the system at the end of the laser pulse is shown in Figure 4 at 50 ps. In contrast to the photochemical system at 50 ps, there are fewer beads above the surface. As time progresses, there continue to be some bond-breaking events due to thermal and mechanical stresses but there is not as much fragmentation as in the simulation with photon-induced bond cleavage. The onset of ablation is delayed longer than for the photochemical process. The ablation process starts at 80 ps; before this there are single particles in the plume. The high temperature in the absorbing region leads to overheating of the material and photothermal bond dissociation. Despite the higher number of photons, the

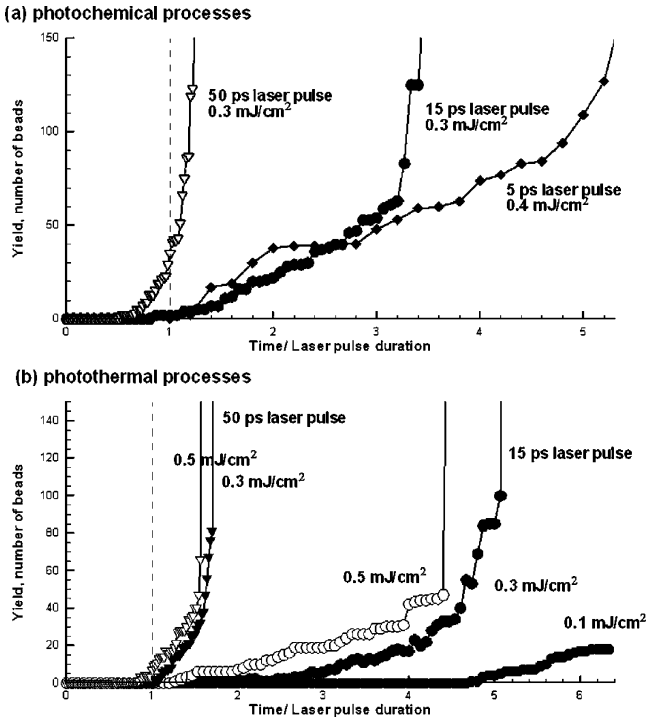

Figure 5. Yield of particles as a function of time/laser pulse with (a) photochemical processes and (b) photothermal processes. The yield is expressed in terms of the number of beads ablating from the surface to give a sense of the total mass removed and is measured in the final positions comparable to the last snapshot of Figures 3 and 4.

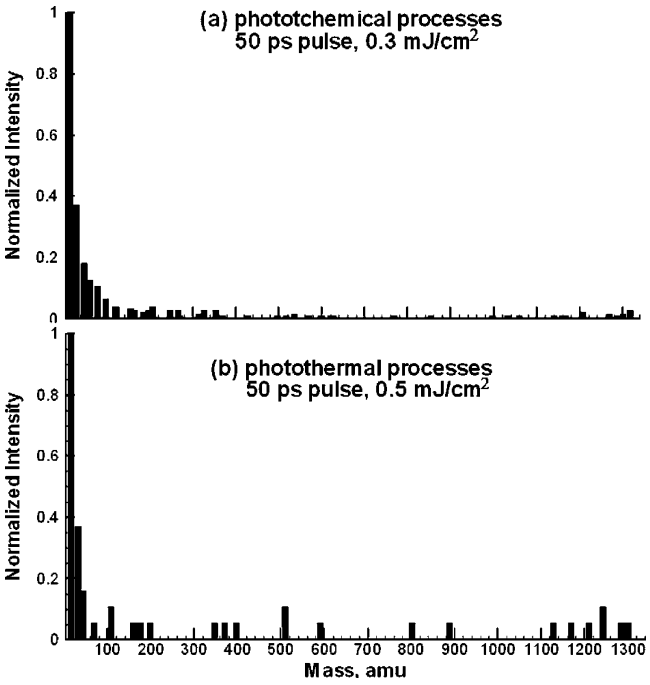

Figure 6. Normalized intensity of emitted particles versus mass for (a) photochemical processes and (b) photothermal processes. One MMA group has a mass of 100 amu. The yields are measured at the final snapshot of Figures 3 and 4.

yield is smaller for the photothermal process than for photochemical one since the number of bonds broken in the former case is smaller.

The time delay for the onset of ablation is observed for both photochemical and photothermal processes. In both cases, the extent of the time delay is dependent on the laser pulse duration and fluence. In Figure 5, the yield of particles versus time relative to the laser pulse is plotted for photochemical and photothermal processes with different laser fluences and pulse widths. The sharp increase in yield indicates the onset of ablation. The cohesive energy per polymer value is smaller for photochemical processes than for photothermal ones, which could be the reason for earlier onset of ablation for photochemical processes. The delay of the onset of ablation versus the laser pulse width is a common observation[78] for photochemical and photothermal processes, which is related to the pressure wave propagation in a stiff and viscous polymer medium.

Another difference in the effect of excitation processes is the plume composition. The calculated mass spectrum of the ejected material is shown in Figure 6. In the case of photochemical processes, the plume consists of small fragments of polymers and several large fragments. The small fragments consist of many terminal CH_3 radicals and fragments of less than two MMA groups. The large fragments consist of intact polymers and polymers minus one MMA group. In the case of photothermal processes, there are many larger fragments of polymers with more than four MMA groups in a polymer.

Several of the observations from the calculations are in agreement with experimental observations. The low surface swelling of doped PMMA samples was observed experimentally for a 193 nm wavelength with 30 ns and 500 fs pulse lengths[79,80] and for 100 ps laser pulses at 266 and 1064 nm[81] wavelengths. Srinivasan et al. reported that chemical changes occurred at the surface during the laser pulse but that the emission process was delayed for 193 nm irradiation.[82] A 20 ps time delay for the onset of PMMA ablation at all laser intensities was observed for 532 nm laser ablation with a 93 ps pulse.[83] The study of laser ablation of a PMMA sample doped with IR-165 at 1064 nm wavelength and 150 ps pulses revealed the "shock-assisted photothermal ablation", where the onset of ablation was determined to be generated by equal contributions from the pressure release and thermochemical decomposition.[84]

Summary and Conclusion

A coarse-grained chemical reaction model has been developed for computer simulations of laser ablation of polymers. The coarse-grained representation of a polymer allows the study of larger systems and longer times, which are essential for laser ablation phenomena. Using a well-balanced blend of experimental information for the basic chemical reactions and a probabilistic occurrence of some events, we are able to perform mesoscopic molecular dynamics simulations of laser ablation of polymers at realistic length and time scales. The centerpiece of the proposed simulations is the ability to include the effect of widespread chemical reactions on the dynamical events. This model is ideal for delineating the nuances of photochemical reactions and their associated composition, volume, and heat changes on the ablation phenomena.

In this paper, the model is applied to the investigation of effects of main chain scission events (Norrish type II reaction) and photothermal excitation of a 3D PMMA sample. In particular, the yield and composition dependence on the fluence and mechanism of excitation has been observed. The yield versus time for various fluences shows that the onset of ablation is delayed with the use of shorter laser pulses. Lower fluence is needed for the onset of ablation with photochemical processes than with photothermal processes. The laser-induced pressure relaxation is the main mechanism responsible for the onset of polymer ablation, the vaporization processes are not efficient, and the effect is minimal for both photochemical and photothermal processes. During the laser pulse, only single particles

and MMA groups are desorbed from the surface; however, the intact polymers are observed in the plume during ablation. Shorter polymer chains are observed in the plume for photochemical processes than for photothermal processes. The model predicts that the critical number density of the broken bonds in the surface layer is achieved by photomechanical processes, splitting the polymer chains in the absorbing region of the material.

Acknowledgment. This work was supported by the U.S. Air Force Office of Scientific Research through the Multi-University Research Initiative and the National Science Foundation through the Information Technology Research program. The computer support was provided by the Academic Services and Emerging Technologies group at Pennsylvania State University.

References and Notes

(1) Kawamura, Y.; Toyoda, K.; Namba, S. *Appl. Phys. Lett.* **1982**, *40*, 374.
(2) Srinivasan, R.; Mayne-Banton, V. *Appl. Phys. Lett.* **1982**, *41*, 576.
(3) Dyer, P. E. *Appl. Phys. A* **2003**, *77*, 167.
(4) Bachmann, F. *Chemtronics* **1989**, *4*, 149.
(5) Lankard, J. R.; Wolbold, G. *Appl. Phys. A* **1992**, *54*, 355.
(6) Brannon, J. H.; Wassick, T. A. *Proc. SPIE-Int. Soc. Opt. Eng.* **1997**, *2991*, 146.
(7) Brannon, J. H.; Tam, A. C.; Kurth, R. H. *J. Appl. Phys.* **1991**, *70*, 3881.
(8) Phillips, H. M.; Callahan, D. L.; Sauerbrey, R.; Szabo, G.; Bor, Z. *Appl. Phys. A* **1992**, *54*, 158.
(9) Pugmire, D. L.; Waddell, E. A.; Haasch, R.; Tarlov, M. J.; Locascio, E. *Anal. Chem.* **2002**, *74*, 871.
(10) Lippert, T.; David, C.; Hauer, M.; Phipps, C.; Kokaun, A. *Rev. Laser Eng.* **2001**, *29*, 734.
(11) Yabe, T.; Phipps, C.; Aoki, K.; Yamaguchi, M.; Nakagawa, R.; Baasandash, C.; Ogata, Y.; Shiho, M.; Inoue, G.; Onda, M.; Horioka, K.; Kajiwara, I.; Yoshida, K. *Appl. Phys. A* **2003**, *77*, 243.
(12) Phipps, C. R.; Luke, J. R.; McDuff, G. G.; Lippert, T. *Appl. Phys. A* **2003**, *77*, 193.
(13) Gorman, C. The laser fix. *TIME*, Vol. 154, October 11, 1999.
(14) Lippert, T.; Dickinson, J. T. *Chem. Rev.* **2003**, *103*, 453.
(15) Lazare, S.; Granier, V. *Laser Chem.* **1989**, *10*, 25.
(16) Deutsch, T. F.; Geis, M. W. *J. Appl. Phys.* **1983**, *54*, 7201.
(17) Andrew, J. E.; Dyer, P. E.; Foster, D.; Key, P. H. *Appl. Phys. Lett.* **1983**, *43*, 717.
(18) Sutcliffe, E.; Srinivasan, R. *J. Appl. Phys.* **1986**, *60*, 3315.
(19) Mahan, G. D.; Cole, H. S.; Liu, Y. S.; Philipp, H. R. *Appl. Phys. Lett.* **1988**, *53*, 2377.
(20) Pettit, G. H.; Ediger, M. N.; Hahn, D. W.; Brinson, B. E.; Sauerbrey, R. *Appl. Phys. A* **1994**, *58*, 573.
(21) Pettit, G. H.; Sauerbrey, R. *Appl. Phys. Lett.* **1991**, *58*, 793.
(22) Pettit, G. H.; Sauerbrey, R. *Appl. Phys. A* **1993**, *56*, 51.
(23) Arnold, N.; Luk'yanchuk, B.; Bityurin, N. *Appl. Surf. Sci.* **1998**, *127*−*129*, 184.
(24) Cain, S. R.; Burns, F. C.; Otis, C. E. *J. Appl. Phys.* **1992**, *71*, 4107.
(25) Cain, S. R. *J. Phys. Chem.* **1993**, *97*, 7572.
(26) D'Couto, G. C.; Babu, S. V. *J. Appl. Phys.* **1994**, *76*, 3052.
(27) Luk'yanchuk, B.; Bityurin, N.; Himmelbauer, M.; Arnold, N. *Nucl. Instrum. Methods Phys. Res., Sect. B* **1997**, *122*, 347.
(28) Schmidt, H.; Ihlemann, J.; Wolff-Rottke, B.; Luther, K.; Troe, J. *J. Appl. Phys.* **1998**, *83*, 5458.
(29) Srinivasan, V.; Smrtic, M. A.; Babu, S. V. *J. Appl. Phys.* **1986**, *59*, 3861.
(30) Luk'yanchuk, B.; Bityurin, N.; Anisimov, S.; Bauerle, D. *Appl. Phys. A* **1993**, *57*, 367.
(31) Luk'yanchuk, B.; Bityurin, N.; Anisimov, S.; Arnold, N.; Bauerle, D. *Appl. Phys. A* **1996**, *62*, 397.
(32) Bityurin, N.; Malyshev, A.; Luk'yanchuk, B.; Anisimov, S.; Bauerle, D. *Proc. SPIE-Int. Soc. Opt. Eng.* **1996**, *2802*, 102.
(33) Bityurin, N. *Appl. Surf. Sci.* **1999**, *138*−*139*, 354.
(34) Srinivasan, R.; Braren, B. *Chem. Rev.* **1989**, *89*, 1303.
(35) Treyz, G. V.; Scarmozzino, R.; Osgood, R. M. *Appl. Phys. Lett.* **1989**, *55*, 346.
(36) Kuper, S.; Brannon, J.; Brannon, K. *Appl. Phys. A* **1993**, *56*, 43.
(37) Arnold, N.; Bityurin, N. *Appl. Phys. A* **1999**, *68*, 615.
(38) Palmer, B. J.; Keyes, T.; Clarke, R. H.; Isner, J. M. *J. Phys. Chem.* **1989**, *93*, 7509.
(39) Gai, H. D.; Voth, G. A. *J. Appl. Phys.* **1992**, *71*, 1415.
(40) Cain, S. R.; Burns, F. C.; Otis, C. E.; Braren, B. *J. Appl. Phys.* **1992**, *72*, 5172.
(41) Sadoqi, M.; Kumar, S.; Yamada, Y. *J. Thermophys. Heat Transfer* **2002**, *16*, 193.
(42) Stoliarov, S. I.; Westmoreland, P. R.; Nyden, M. R.; Forney, G. P. *Polymer* **2003**, *44*, 883.
(43) Zhigilei, L. V.; Kodali, P. B. S.; Garrison, B. J. *J. Phys. Chem. B* **1997**, *101*, 2028.
(44) Zhigilei, L. V.; Garrison, B. J. *J. Appl. Phys.* **2000**, *88*, 1281.
(45) Yingling, Y. G.; Zhigilei, L. V.; Garrison, B. J. *J. Photochem. Photobiol., A* **2001**, *145*, 173.
(46) Yingling, Y. G.; Garrison, B. J. *Chem. Phys. Lett.* **2002**, *364*, 237.
(47) Yingling, Y. G.; Garrison, B. J. *J. Phys. Chem. B* **2004**, *108*, 1815.
(48) Zhigilei, L. V.; Leveugle, E.; Garrison, B. J.; Yingling, Y. G.; Zeifman, M. I. *Chem. Rev.* **2003**, *103*, 321.
(49) Zhigilei, L. V.; Yingling, Y. G.; Itina, T. E.; Schoolcraft, T. A.; Garrison, B. J. *Int. J. Mass Spectrom.* **2003**, *226*, 85.
(50) Yingling, Y. G.; Garrison, B. J. *Nucl. Instrum. Methods Phys. Res., Sect. B* **2003**, *202*, 188.
(51) Yingling, Y. G.; Zhigilei, L. V.; Garrison, B. J. *Nucl. Instrum. Methods Phys. Res., Sect. B* **2001**, *180*, 171.
(52) Itina, T. E.; Zhigilei, L. V.; Garrison, B. J. *J. Phys. Chem. B* **2002**, *106*, 303.
(53) Yingling, Y. G.; Zhigilei, L. V.; Garrison, B. J.; Koubenakis, A.; Labrakis, J.; Georgiou, S. *Appl. Phys. Lett.* **2001**, *78*, 1631.
(54) Zhigilei, L. V.; Garrison, B. J. *Appl. Phys. Lett.* **1997**, *71*, 551.
(55) Zhigilei, L. V.; Garrison, B. J. *Rapid Commun. Mass Spectrom.* **1998**, *12*, 1273.
(56) Ochiai, Y.; Baba, M.; Watanabe, H.; Matsui, S. *Jpn. J. Appl. Phys., Part 1* **1991**, *30*, 3266.
(57) Li, Y.; Yamada, K.; Ishizuka, T.; Watanabe, W.; Itoh, K.; Zhou, Z. X. *Opt. Express* **2002**, *10*, 1173.
(58) Jacobsen, C.; Howells, M.; Kirz, J.; Rothman, S. *J. Opt. Soc. Am. A* **1990**, *7*, 1847.
(59) Kunz, R. R.; Downs, D. K. *J. Vac. Sci. Technol., B* **1999**, *17*, 3330.
(60) Garino, J. P.; Nazarian, D.; Froimson, M. I.; Grelsamer, R. P.; Treat, M. R. *Proc. SPIE-Int. Soc. Opt. Eng.* **1991**, *1424*, 43.
(61) Sazy, J.; Kollmer, C.; Uppal, G. S.; Lane, G. J.; Sherk, H. H. *Proc. SPIE-Int. Soc. Opt. Eng.* **1991**, *1424*, 50.
(62) Naessens, K.; Van Daele, P.; Baets, R. *Microlens fabrication in PMMA with scanning excimer laser ablation technique*, Proceeding Symposium IEEE/LEOS Benelux Chapter, Delft University of Technology: The Netherlands, 2000, ISBN: IS90900142606.
(63) Rizvi, R. H. *RIKEN Rev.* **2003**, *50*, 107.
(64) Anschutz, T.; Pieger, S. *J. Refract. Surg.* **1999**, *15*, S252.
(65) Lade, R. J.; Morley, I. W.; May, P. W.; Rosser, K. N.; Ashfold, M. N. R. *Diamond Relat. Mater.* **1999**, *8*, 1654.
(66) Krebs, H.-U.; Weisheit, M.; Faupel, J.; Süske, E.; Scharf, T.; Fuhse, C.; Störmer, M.; Sturm, K.; Seibt, M.; Kijewski, H.; Nelke, D.; Panchenko, E.; Buback, M. *Adv. Solid State Phys.* **2003**, *43*, 505.
(67) Fedynyshyn, T. H.; Kunz, R. R.; Sinta, R. F.; Goodman, R. B.; Doran, S. P. *J. Vac. Sci. Technol., B* **2000**, *18*, 3332.
(68) Zhang, X.; Jacobsen, C.; Lindaas, S.; Williams, S. *J. Vac. Sci. Technol., B* **1995**, *13*, 1477.
(69) Shalaby, S. W. *Radiation Effects on Polymers*; ACS Symposium Series; American Chemical Society: Washington, DC, 1991.
(70) Harbron, E. J.; McCaffrey, V. P.; Xu, R. X.; Forbes, M. D. E. *J. Am. Chem. Soc.* **2000**, *122*, 9182.
(71) Conforti, P. F.; Garrison, B. J. *Chem. Phys. Lett.* **2005**, *406*, 294.
(72) Cascales, J. J. L.; Díaz, F. G.; de la Torre, J. G. *Polymer* **1995**, *36*, 345.
(73) Soldera, A. *Polymer* **2002**, *43*, 4269.
(74) Kim, W. K.; Hayden, L. M. *J. Chem. Phys.* **1999**, *111*, 5212.
(75) Tsai, J.; Taylor, R.; Chothia, C.; Gerstein, M. *J. Mol. Biol.* **1999**, *290*, 253.
(76) Zhigilei, L. V.; Garrison, B. J. *Mater. Res. Soc. Symp. Proc.* **1999**, *538*, 491.
(77) Srinivasan, R.; Leigh, W. J. *J. Am. Chem. Soc.* **1982**, *104*, 6784.
(78) Dyer, P. E.; Srinivasan, R. *Appl. Phys. Lett.* **1986**, *48*, 445.
(79) Athanassiou, A.; Andreou, E.; Anglos, D.; Georgiou, S.; Fotakis, C. *Appl. Phys. A* **1999**, *69*, S285.
(80) Athanassiou, A.; Andreou, E.; Fragouli, D.; Anglos, D.; Georgiou, S.; Fotakis, C. *J. Photochem. Photobiol., A* **2001**, *145*, 229.
(81) Hahn, C.; Lippert, T.; Wokaun, A. *J. Phys. Chem. B* **1999**, *103*, 1287.
(82) Srinivasan, R.; Braren, B.; Casey, K. G.; Yeh, M. *Appl. Phys. Lett.* **1989**, *55*, 2790.
(83) Zyung, T.; Kim, H.; Postlewaite, J. C.; Dlott, D. D. *J. Appl. Phys.* **1989**, *65*, 4548.
(84) Hare, D. E.; Franken, J.; Dlott, D. D. *J. Appl. Phys.* **1995**, *77*, 5950.